



Contents lists available at ScienceDirect

# Waste Management

journal homepage: [www.elsevier.com/locate/wasman](http://www.elsevier.com/locate/wasman)

## Irradiated recycled plastic as a concrete additive for improved chemo-mechanical properties and lower carbon footprint

Carolyn E. Schaefer<sup>a</sup>, Kunal Kupwade-Patil<sup>b,\*</sup>, Michael Ortega<sup>a</sup>, Carmen Soriano<sup>c</sup>, Oral Büyüköztürk<sup>b,\*</sup>, Anne E. White<sup>a</sup>, Michael P. Short<sup>a,\*</sup>

<sup>a</sup> Department of Nuclear Science and Engineering, Massachusetts Institute of Technology, Cambridge, MA 02139, USA

<sup>b</sup> Department of Civil and Environmental Engineering, Massachusetts Institute of Technology, Cambridge, MA 02139, USA

<sup>c</sup> Advance Photon Source (APS), Argonne National Laboratory, 9700 South Cass Ave, Lemont, IL 60439, USA

### ARTICLE INFO

#### Article history:

Received 19 June 2017

Revised 19 September 2017

Accepted 27 September 2017

Available online xxxx

#### Keywords:

Irradiated plastic

Additives

Cement paste

Microstructure

Pore structure

### ABSTRACT

Concrete production contributes heavily to greenhouse gas emissions, thus a need exists for the development of durable and sustainable concrete with a lower carbon footprint. This can be achieved when cement is partially replaced with another material, such as waste plastic, though normally with a tradeoff in compressive strength. This study discusses progress toward a high/medium strength concrete with a dense, cementitious matrix that contains an irradiated plastic additive, recovering the compressive strength while displacing concrete with waste materials to reduce greenhouse gas generation. Compressive strength tests showed that the addition of high dose (100 kGy) irradiated plastic in multiple concretes resulted in increased compressive strength as compared to samples containing regular, non-irradiated plastic. This suggests that irradiating plastic at a high dose is a viable potential solution for regaining some of the strength that is lost when plastic is added to cement paste. X-ray Diffraction (XRD), Backscattered Electron Microscopy (BSE), and X-ray microtomography explain the mechanisms for strength retention when using irradiated plastic as a filler for cement paste. By partially replacing Portland cement with a recycled waste plastic, this design may have a potential to contribute to reduced carbon emissions when scaled to the level of mass concrete production.

© 2017 Elsevier Ltd. All rights reserved.

## 1. Introduction

The use of recycled plastics in concrete has been explored as a means of improving concrete's mechanical properties while also providing an efficient way to both repurpose waste plastic and partially displace cement for the purpose of reducing carbon emissions. The task remains, however, to develop a cement design that allows for both the addition of plastic and the preservation of high compressive strength. This study explores the effectiveness of gamma-irradiated plastic as an additive in cement paste (Portland cement + additives + water) samples for improving the compressive strength. Irradiated plastic is paired with different mineral additives, which are commonly used to achieve high strength, with the goal of finding an optimal combination. An internal microstructure analysis is presented in order to provide some insight into the aspects of the materials' chemical compositions that contribute to the observed variation in strength. The

objective is to determine whether or not irradiated plastic is an effective partial replacement for cement; achieving a high/medium-strength concrete using this additive would imply the ability to produce a lower carbon footprint concrete variety that could even act as a permanent storage option for plastic waste.

### 1.1. Carbon emissions in the cement industry

Concrete is the second most widely used material on the planet, after water (Crow, 2008). The cement industry accounts for roughly 5% of global anthropogenic carbon dioxide emissions, making it a critical sector for emission mitigation (Worrell et al., 2001). The production of Portland cement releases carbon dioxide both directly and indirectly (Ali et al., 2011; Tanaka and Stigson, 2009). Direct emissions result from a process known as calcination, which occurs when limestone, the primary component of cement, is heated (Andres et al., 1996). The calcium carbonate in the limestone breaks down into calcium oxide and carbon dioxide (Taylor, 1997). This process accounts for roughly half of all emissions from cement production. To produce cement, limestone and other clay-like materials are heated in a kiln at around 1400 °C. Indirect

\* Corresponding authors.

E-mail addresses: [kunalk@mit.edu](mailto:kunalk@mit.edu) (K. Kupwade-Patil), [obuyuk@mit.edu](mailto:obuyuk@mit.edu) (O. Büyüköztürk), [hereiam@mit.edu](mailto:hereiam@mit.edu) (M.P. Short).

emissions result from the burning of fossil fuels to heat the kiln and account for about 40% of cement production emissions. The electricity used to power additional plant machinery, as well as the final transportation of cement, account for the remaining 10% of total emissions. These emissions make partial replacement of cement with a substitute material an attractive alternative to alleviate the negative environmental impact of cement production.

### 1.2. Plastic waste and recycling

Constituting a separate environmental issue is the abundance of plastic waste. Plastics have come to play an essential role in our everyday lives. Their favorable properties, including low cost, high strength-to-weight ratio, and low density make them ideal for use in a wide range of products (Gu and Ozbaakkaloglu, 2016; Singh et al., 2017). It has been shown that over half of global plastic production is used for one-off disposable consumer products. This contributes heavily to the production of plastic-related waste, most of which is not biodegradable and will not react chemically in natural settings, and therefore it remains in the environment for decades or even centuries. Plastic wastes have become universally accepted as a serious environmental issue.

Despite improvements in technology and awareness that have occurred since the recycling of plastic waste began in 1980, the recycling rate of post-consumed plastic wastes is still fairly low (EPA, 2014). A 2012 study showed a plastic recycling rate of only 8.8%, while the remaining 91.2% was simply discarded. The discarded plastic is typically put into a landfill, which is considered the least desirable method of dealing with plastic waste because it demands heavy space consumption and contributes to long-term pollution (EPA, 2014; Gu and Ozbaakkaloglu, 2016). In some countries waste plastic is incinerated for energy recovery because of its high calorific value. This method, however, produces toxic ash and releases carbon dioxide and poisonous chemicals into the environment. Recycling, therefore, is seen as the ideal solution for minimizing environmental impact. Among the various approaches to managing recycling are (1) standard mechanical recycling, which aims to recover plastic via mechanical processes (sorting, grinding, cleaning, drying, re-granulating, etc.) and produces recyclates that can be transformed into new plastic products, and (2) recycling in the form of repurposing the waste plastic without fully breaking it down (Al-Salem et al., 2009). Mechanical recycling degrades the quality of the plastic during the service cycle, and often times the plastic that is recycled in the United States is exported, with about two-thirds being shipped to China (Gu and Ozbaakkaloglu, 2016). This is due to the fact that the U.S. recycling market is small in comparison to other countries (Yoshida, 2005). The exported plastic is shipped overseas via massive cargo ships, which collectively release billions of tons of CO<sub>2</sub> annually, along with considerable amounts of nitrogen and sulfur (Corbett and Fischbeck, 1997). Thus reusing waste plastic in other industries is considered a more ideal method of disposal (Gu and Ozbaakkaloglu, 2016).

### 1.3. Plastic as an additive in concrete

The use of a wide range of plastics as additives to concrete, in the form of powder, aggregate and fiber, has been extensively studied by several researchers (Asokan et al., 2010; Choi et al., 2009; Gesoglu et al., 2017; Kim et al., 2010; Siddique et al., 2008). Recently, researchers have explored waste and recycled plastic's potential as an environmentally friendly construction material by repurposing it as an additive in concrete mix and studying the concrete's resultant behavior (Gu and Ozbaakkaloglu, 2016). Specifically, polyethylene terephthalate (PET) has been explored as a lightweight concrete aggregate that could improve various

mechanical properties and replace the standard lightweight aggregates that are typically used, which face some problems related to both cost and quality (Choi et al., 2005). A recent study shows that manufactured plastic aggregate can be used at 25% replacement level for natural aggregates while providing a benefit of light weight aggregate concrete subsequently maintaining the required strength and ductility for non-structural applications (Alqahtani et al., 2017). Another work demonstrates that plastic from bottles shredded into small PET particulates was successfully used as sand-substitution aggregates in cementitious concrete composites (Marzouk et al., 2007). Moreover, use of plastic aggregates from foam-extrusion process has led to improved aggregate/binder interface, and reduction in dead-weight of the structure and overall reduction in consumption of natural sand (Coppola et al., 2016). Also, inclusion of plastic as an aggregate can lead to significant reduction in the thermal conductivity subsequently improving the thermal insulation performance of the mortars (Colangelo et al., 2016; Iucolano et al., 2013). Plastic aggregates have five times lower thermal conductivity than silica based aggregated which can be used to control the heat loss from buildings during summer and heat gain in the winter. For detailed review on usage of waste plastic as an aggregate in mortar and concretes the readers are referred to a state of art review article by Saikia and de Brito (2012).

PET is a polymer notable for being the constituent of the clear plastic used for soda and water bottle containers. In comparison to Polypropylene (PP) and polyethylene (PE), PET in concrete can improve the concrete's flexural toughness, impact resistance, and workability (Choi et al., 2005; Kim et al., 2010; Pelisser et al., 2012). Moreover, PET is highly sensitive to the alkaline environment in the pore solution of cementitious matrix, which can act as a precursor that can contribute to dense forming phases. Various studies have shown mixed results for improvements in tensile strength (Saikia and Brito, 2013). Compressive strength, however, has generally been shown to decrease with the addition of PET. Thus it is apparent that the task remains to produce a PET-enhanced concrete capable of demonstrating the aforementioned mechanical improvements without compromising its compressive strength.

### 1.4. Gamma irradiation of PET

One potential solution for recovering some of the strength back that is lost when plastic is added to concrete is to make use of irradiation to improve the concrete's strength properties (Martínez-Barrera et al., 2006, 2011, 2005). PET is a semi-crystalline polyester that exhibits an isotropic microstructure due to its glassy amorphous composition (Jog, 1995). For this reason, it is one of the most studied polymers. Upon irradiation, the two effects of greatest importance for PET are chain scission and crosslinking (Plester, 1973). It has been shown that, due to the chain scission effect, the degree of crystallinity in PET increases with gamma radiation dose (Kattan, 2006). The number of chain scissions increases with dose, thereby decreasing the molecular weight. This reduced weight accounts for improved molecular mobility, which facilitates the ordered arrangement of molecules in crystalline structures. Thus the increase in mobility as a result of chain scission leads to greater crystallizability when PET is irradiated by gamma rays. The extent of crystallinity has a significant impact on several mechanical properties of PET (Demirel et al., 2016). Higher crystallinity PET has been shown to have higher modulus, toughness, stiffness, strength, and hardness. Alternatively, crosslinking is the chemical bonding of one polymer chain to another (Plester, 1973). It can be induced by radiation and has the effect of strengthening the chemical structure of the compound. Thus both chain

scission and crosslinking (which can occur simultaneously) in PET can result in its improved strength.

### 1.5. Industrial byproducts as current high strength options

Industrial byproducts such as silica fume, a byproduct of silicon production, and fly ash, a byproduct of coal combustion are commonly used to enhance concrete strength and water permeability characteristics (Muhit et al., 2013). This is useful both for creating High Performance Concrete and for minimizing the potential hazardous effects these byproducts have on the environment. These additives, when used in a concrete admixture, combine with calcium hydroxide liberated during cement hydration to form additional calcium silicate hydrate (C–S–H), the glue that strengthens and holds concrete together (Roy et al., 2001). This additional C–S–H densifies the cementitious matrix, thereby enhancing strength. When used to partially replace OPC in cement mixtures, these supplementary cementitious materials act to decrease water penetration and improve concrete's compressive and tensile strength considerably, thus creating a feasible alternative for fabricating sustainable and durable cementitious materials.

### 1.6. Research objective and justification of this study

A cement mix design that allows for both the addition of waste plastic and the preservation of high compressive strength remains to be discovered. This research aims to examine the effectiveness of irradiated plastic as an additive for enhancing the mechanical properties of concrete. Because gamma irradiation of PET is known to result in a strengthened chemical structure, there is reason to believe that an irradiated waste plastic additive would take advantage of the improvements in concrete's mechanical properties due to plastic alone as well as the polymer strength improvements resulting from irradiation. The collective effects are likely to provide a better solution than either contribution might achieve on its own. Within this scope is an additional objective of understanding the effect of the waste plastic's radiation dose on concrete strength by examining the effect of dosage on the cementitious matrix itself. Furthermore, because the addition of an industrial byproduct is necessary to achieve high strength concrete, this work seeks to optimize the combination of both additive types—plastic and either fly ash or silica fume—by testing a series of dose–byproduct pairings for improved compressive strength. Phase identification through X-ray diffraction (XRD) analysis, imaging through backscattered electron microscopy (BSE), and pore structure analysis via 3D imaging through X-ray micro computed tomography are utilized to collectively assess the internal structure of the samples and to help determine which aspects of the materials' compositions contribute to variability in strength and porosity. This multiscale approach is used to characterize the complex matrix developed within the cement due to the addition of both additive types.

As discussed in Section 1.1, the manufacture of Portland cement is an energy intensive process that releases large amounts of carbon dioxide into the atmosphere. In the design presented here, the sample compositions are such that the plastic additive displaces a fraction of OPC. Because OPC production contributes so heavily to carbon emissions, achieving a high-strength concrete using an irradiated plastic additive would provide a solution that not only takes advantage of the known mechanical improvements resulting from the addition of plastic but also serves as a lower carbon footprint concrete variety that could even act as a permanent storage option for plastic waste.

## 2. Materials and methods

A series of cement paste samples were prepared, each with a different combination of mineral additive and plastic irradiation dose. Cement paste samples were prepared using a water to cement ratio of 0.35 using Type I Portland cement and Class F fly ash and silica fume were included as supplementary cementitious materials (SCM). After a 28-day cure period, these specimens underwent compression testing to determine the variation in their strengths (ASTM-C109, 2016). To assess the internal structure of the cement paste microstructure and gain some insight into what aspects of their compositions contributed to the observed strength differences, a microstructural analysis—consisting of XRD, Backscattered Electron Spectroscopy/Energy Dispersive Spectrum (BSE/EDS), and X-ray micro tomography was performed.

### 2.1. Mix design for cement paste

The complete mix design for the concrete samples is shown in Table 1. Included are three different cement binders: Type I Ordinary Portland Cement (OPC), OPC with Class F fly ash (OPC+FA), and OPC with silica fume (OPC+SF). For each binder, there were low-dose, high-dose, and no-dose combinations. Each individual combination was triplicated so that an average compressive strength with an uncertainty could ultimately be determined. For each of the non-control samples, the plastic made up 1.25% of the dry mass (see Appendix A for justification of this percent composition). Studies show no improvements in concrete compressive strength for plastic composition beyond 1.5% by volume, hence 1.25% composition by weight was selected for the current study (Batayneh et al., 2007; Hannawi et al., 2010; Nibudey et al., 2013; Rai et al., 2012). For samples containing both the plastic additive and one of the mineral additives as the binder, the plastic only displaced the cement dry mass; the mineral additive consistently made up 15% of the total dry mass.

### 2.2. X-Ray fluorescence (XRF) spectroscopy and particle size distribution (PSD) analysis

The chemical compositions of OPC, Class F fly ash, and silica fume were measured using X-Ray fluorescence (XRF) spectroscopy. The results are shown in Table 2. The sum of silicon oxide ( $\text{SiO}_2$ ), aluminum oxide ( $\text{Al}_2\text{O}_3$ ), and ferric oxide ( $\text{Fe}_2\text{O}_3$ ) components for the fly ash is 90.01%, indicating that this material is a Class F type of ash according to ASTM C 618 (ASTM, 2004). Particle size distribution (PSD) was conducted on all three materials by suspending them in isopropyl alcohol using a Laser Light Scattering technique with a particle size analyzer. The mean particle sizes for OPC, Class F fly ash, and silica fume were found to be 12.73, 38.50, and 12.05  $\mu\text{m}$ , respectively.

### 2.3. Preparation of irradiated plastic additive

For considerations of dose level in the context of this design, previous studies were used to determine the effect of gamma irradiation on the strength properties of plastic at varying doses. Literature review showed that different types of strength were maximized in different dose ranges (Plester, 1973). These dose–strength relationships are summarized in Appendix B. Specifically, one study showed that tensile strength increased up to 10 kGy (Plester, 1973), while another reported that radiation-induced crosslinking improved strength for doses up to 150 kGy (Martínez-Barrera et al., 2015). Consequently, it was decided that a high dose of 100 kGy and a low dose of 10 kGy should be tested

**Table 1**  
Mix design of the cement paste samples.

Notation	Binder	Type	Total dry mass (g)	Plastic (g)	OPC (g)	Class F fly ash (g)	Silica fume (g)
OPC-Ctrl	OPC	Ctrl	1400	0	1400	0	0
OPC-RP	OPC	RP	1400	17.5	1382.5	0	0
OPC-HD	OPC	HD	1400	17.5	1382.5	0	0
OPC-LD	OPC	LD	1400	17.5	1382.5	0	0
FA-Ctrl	OPC+FA	Ctrl	1400	0	1190	210	0
FA-RP	OPC+FA	RP	1400	17.5	1172.5	210	0
FA-HD	OPC+FA	HD	1400	17.5	1172.5	210	0
FA-LD	OPC+FA	LD	1400	17.5	1172.5	210	0
SF-Ctrl	OPC+SF	Ctrl	1400	0	1190	0	210
SF-RP	OPC+SF	RP	1400	17.5	1172.5	0	210
SF-HD	OPC+SF	HD	1400	17.5	1172.5	0	210
SF-LD	OPC+SF	LD	1400	17.5	1172.5	0	210

FA = Fly ash, SF = Silica fume, Ctrl = No plastic, RP = Regular plastic, HD = High dose plastic, LD = Low dose plastic; Water to Binder Ratio = 0.35.

**Table 2**  
Mass% of oxide composition of the Portland cement, class F fly ash and silica fume.

Chemical composition (mass % of oxide)	CaO	SiO <sub>2</sub>	Al <sub>2</sub> O <sub>3</sub>	MgO	SO <sub>3</sub>	TiO <sub>2</sub>	K <sub>2</sub> O	Fe <sub>2</sub> O <sub>3</sub>	Na <sub>2</sub> O	MnO	SrO	Mean Particle Size (μm)
<i>Binder type</i>												
OPC	62.27	16.63	3.63	1.22	3.91	0.24	0.61	3.28	0.34	0.06	0.07	12.73
Class F FA	3.82	61.72	19.07	1.57	0.25	2.44	1.27	9.22	0.68	—	—	38.50
SF	1.2	85.50	1.61	1.4	0.40	<0.05	0.65	1.89	0.43	0.01	0.01	12.05

SF = Silica Fume, FA = Fly Ash, OPC = Ordinary Portland cement (OPC).

and compared. These levels determine the length of irradiation time for the desired high- and low-dose plastic additives.

Plastic flakes obtained from a recycling facility were used for the plastic additive. Due to imperfections in recycling facilities' sorting processes, the sample originally contained pieces of metal and other non-plastic impurities. In an effort to eliminate the possibility that these impurities would contaminate or ruin the future cement samples, the plastic was manually sorted to remove all materials that were clearly not plastic. Half of the plastic was then irradiated in a cobalt-60 irradiator facility that operates at 58 Gy/min. The low dose sample was left in the machine for 2.9 h for a total of 10 kGy. The high dose sample was left in the machine for 28.7 h for a total dose of 100 kGy. The flakes were then further crushed using both a high-energy ball mill and a mortar and pestle. Previous studies have shown that the compressive strength of PET-enhanced cement decreases with PET particle size (for samples with a 28-day cure) (Ávila Córdoba et al., 2013). The objective for the crushing process was therefore to achieve a particle size that was as small as possible. Each 18-gram sample was processed for 2 h in the ball mill followed by 20 min with the mortar and pestle. The actual particle size at the end of the process was not uniform, and an average particle size of 170 μm was measured using an optical microscope.

The effect of the irradiation process on the PET's amorphous content was determined by calculating the amorphous and crystalline contributions for each of the three plastic types: high dose, low dose, and no dose. Powder X-ray diffraction (XRD) provides a means of determining the relative amorphous content for most materials. XRD was performed on all three plastics (see Section 2.5.2 for XRD preset specifications and experimental setup, which were the same for the plastics and the cement samples). To quantify the amorphous contribution, High Score Plus software from Pan Analytical was used to analyze the diffraction patterns. The quantification technique used was taken from Klug and Alexander (1974). This method is illustrated in Fig. 1. Though this quantification method does not necessarily produce absolute results, it allows for a batch-to-batch comparison for observing trends in the amorphous content. As shown, the crystalline portion appears to increase with

dose, with the high-dose plastic showing roughly 48% crystallinity.<sup>1</sup> This trend in dose-crystallinity relationship was consistent with expectation (see Section 1.4). The increased crystallinity may have contributed to the higher strengths that were observed in the specimens containing irradiated plastic (see Section 3.1).

#### 2.4. Preparation of cement paste samples

Cement paste samples were constructed using a basic process in which the components were mixed with a kitchen mixer and poured into 2 in. by 4 in. cylindrical molds, a standard for compressive strength testing. A constant water to cement ratio of 0.35 was used for preparing all the samples and mixing procedure was performed as per ASTM C305 (ASTM, 2014). After 24 h, the samples were removed from the molds and placed in tubs of water where they cured for 28 days. Curing is necessary to maintain moisture levels inside cement so that hydration can continue. Once fully cured, the samples were submerged in acetone for 48 h in order to retard the hydration process.

#### 2.5. Methods

##### 2.5.1. Compression testing

Compressive strength testing is a common performance measure for concrete; it provides immediate information on the bulk strength of the specimen being tested. It is also an essential step for gaining critical insight into the potential qualitative relationship between the desirable characteristics of concrete and its strength (Neville, 2011). The specimens were subjected to a compression test as per ASTM C 39 (ASTM, 2016). A 0.20 MPa/s loading rate was selected and kept consistent throughout the testing

<sup>1</sup> A Rietveld analysis was originally planned for quantification of the amorphous content. Thus the plastic samples also contained 10% by weight of corundum powder. The nature of the diffraction patterns made them more suited for the graphical approach used, but it should be noted that the values obtained for the amorphous and crystalline contents in all three plastic are due in part to the 10% by weight inclusion of the corundum.

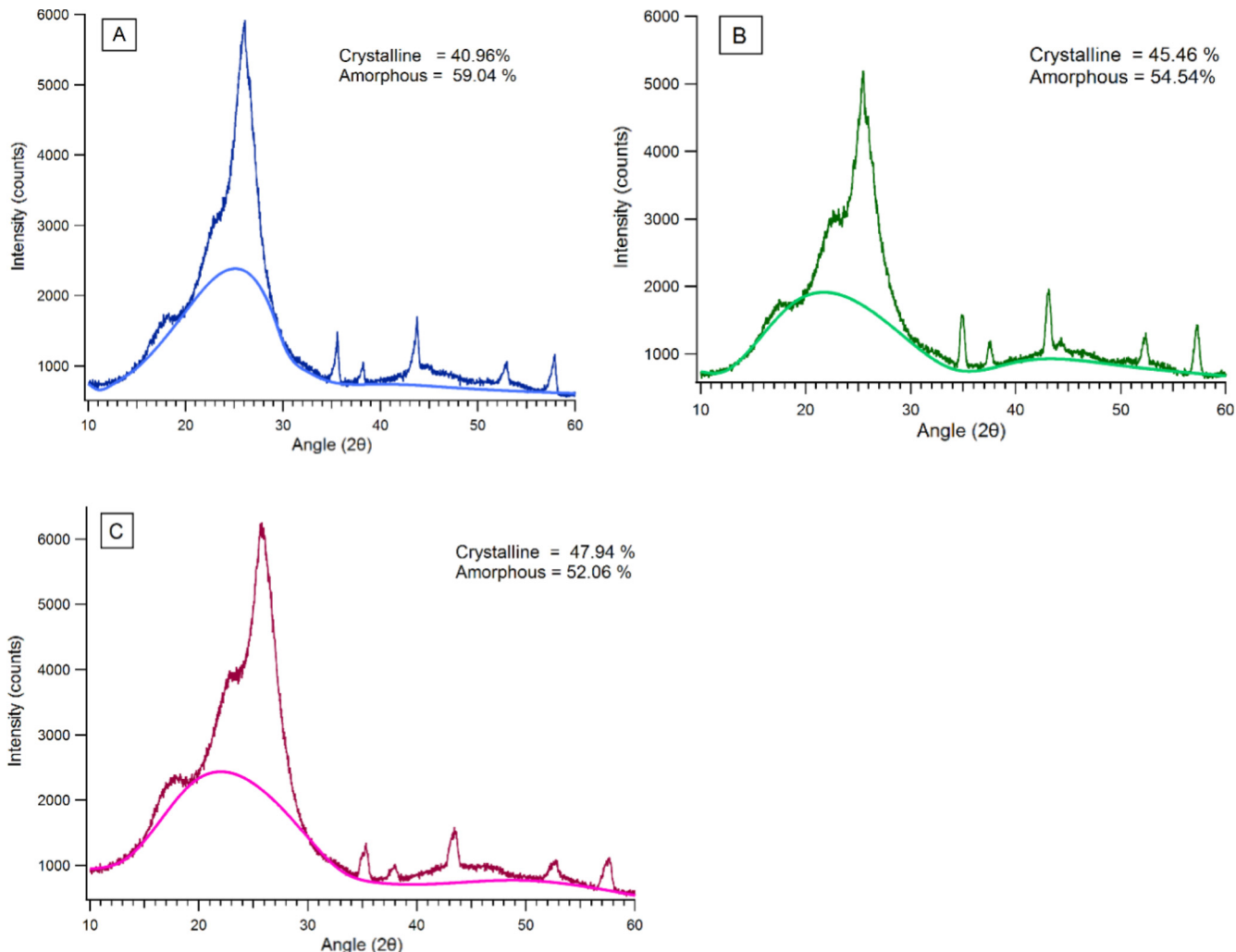


**Fig. 1.** Crystalline and amorphous values obtained for (a) regular plastic, (b) plastic exposed to low dose and (c) plastic exposed to high dose. In the technique applied, the user discriminates between the gradual baseline changes due to the amorphous content (shown by the lighter colored lines) and the background scatter so that the portion above the baseline that separates the crystalline from the amorphous components can be subtracted out, and the diffraction intensity for the amorphous content alone can be determined (Varlashkin, 2011).

procedure. (ASTM C 39 regulates 0.15–0.25 MPa/s as the standard rate for cylindrical specimens (ASTM, 2016; Li, 2011). The percentage of error for the loads within the proposed range of use of the testing machine did not exceed 1.0% of the indicated load (ASTM-C39, 2016). This procedure was performed for each of the three samples of the twelve cement-plastic combinations.

#### 2.5.2. X-Ray Diffraction (XRD)

The specimens, fractured from compression testing, were crushed into a powder so that XRD could be performed for the purpose of identifying and quantifying crystalline phases that might be contributing to the observed variation in strength. The highest strength sample of the three for each of the twelve additive combinations was used for this portion of the study (and for all remaining portions). XRD was conducted with an X-ray diffractometer that uses a Cu-K $\alpha$  radiation nickel foil filter. The ground sample was placed on Bragg–Brentano geometry optics on a flat plate sample geometry. A fixed divergence slit of 1/16° was chosen to limit beam overflow on the samples at small angles of 2 h. Incident and diffracted-side soller slits of 0.02 rad were used for this experiment. The X'Celerator high-speed linear detector was used with an active length of 2.122° 2 h, a step size of 0.0167113° 2 h, and a scan range from 4 to 90°. High Score Plus software from Pan Analytical

was used to carry out the semi-qualitative studies via phase recognition analysis (Scrivener et al., 2016).

#### 2.5.3. Backscattered Electron (BSE) and Energy Dispersive Spectroscopy (EDS) analysis

Backscattered Electron (BSE) imaging was performed on polished samples to examine the additives' effect on the structure and chemistry of the cementitious matrix. For polishing, small fragments from the cement paste samples were epoxy impregnated and polished to 50 nm surface roughness. In BSE, beam electrons are reflected from the sample via elastic scattering. The images created can provide essential information about the distribution of various elements within the sample. A field-emission scanning electron microscope (FE-SEM) by Zeiss was used to carry out the BSE analysis. EDS elemental- and phase-mapping were also carried out on these samples. EDS is a technique used for the chemical characterization that derives its analytical capabilities from measurement of the photon energy emitted from the specimen. Because each element has a unique atomic structure, and therefore a unique electromagnetic emission spectrum, it is possible to characterize individual elements and phases through EDS. Elemental- and phase-maps for each of the twelve polished samples were acquired using this technique.

#### 2.5.4. X-Ray Microtomography (X-Ray $\mu$ CT)

Fragments of the hardened cement paste samples were prepared as approximately 1 mm length cubes and examined using X-ray microtomography at Beamline 2-BM at the Advanced Photon Source, Argonne National Laboratory. X-ray microtomography allows for a full three-dimensional visualization of the samples by combining a series of two-dimensional images. The experimental setup is shown in Fig. 2. Measurements were carried out with a parallel beam configuration using a hard X-ray synchrotron radiation of 25 keV. The samples were mounted between polymeric cones to permit alignment, and all the samples were within the field of view in the horizontal plane of the detector, as shown in Fig. 2. X-ray detection was obtained with a scintillator and a charge coupled device (CCD) camera with a resolution of  $1920 \times 1200$  pixels and a voxel resolution of  $5.86 \mu\text{m}$ . It was coupled to two different Zeiss lenses ( $\times 2.5$  and  $\times 5$  magnification), resulting in scans of  $2.09$  and  $1.08 \mu\text{m}$  of pixel size, and it consisted of 4501 projections obtained through  $180^\circ$  rotation, with a variable exposure time of  $0.2\text{--}0.4$  s, depending on the size of the sample.

A major advantage of X-ray microtomography lies in the ability to extract the three-dimensional morphology of the pore network, which allows for the determination of segmented and effective porosity for the samples. Segmented porosity is associated with the extracted pore space without any consideration of connectivity, whereas effective porosity is the sum total of the interconnected pore space. As an example, Fig. 3 shows a two-dimensional slice of the complete tomographic reconstruction of a representative sample, which was prepared with the OPC+FA-Ctrl sample. Additional image analysis and segmentation using ImageJ 1.48 software were performed in order to calculate the porosity, as detailed in Section 3.4.

### 3. Results and discussion

#### 3.1. Compression test analysis

The results of compression testing for all samples are shown in Fig. 4. Through comparison of the first three bars, which represent the controls, it is clear that the inclusions of fly ash and silica fume alone contributed to increases in strength of 36% and 14%, respectively, as compared to the OPC control. As expected, for all three binder types the inclusion of regular plastic resulted in strengths significantly lower than those of the plastic-free controls. It is interesting to note that inclusion of high dose irradiated plastic in all three binder types (OPC-HD, FA-HD, SF-HD) resulted in increased compressive strength as compared to the samples containing non-irradiated plastic (OPC-RP, FA-RP, SF-RP). This effect was most drastic for OPC samples, for which the addition of high dose irradiated plastic (OPC-HD) contributed to an increase in strength of 20% as compared to OPC-RP. This consistent increase can be attributed in part to the increase in crystallinity of the PET due to irradiation, as shown in Fig. 1.

The effect of the mineral additives alone on compressive strength was also demonstrated, as the inclusion of fly ash led to the highest strengths for all four plastic conditions (Ctrl, RP, LD, HD), followed by silica fume samples. The OPC samples showed the lowest strength for all four plastic conditions. Thus the additional calcium silicate hydrate (C-S-H) formation, which contributes to strength increases, is likely due to the inclusion of both additive types: the mineral additives and the irradiated plastic. The results presented in further sections detail this phase formation using XRD and EDS (via BSE) analysis; they serve to provide a microstructural insight into this variation in compressive strength.

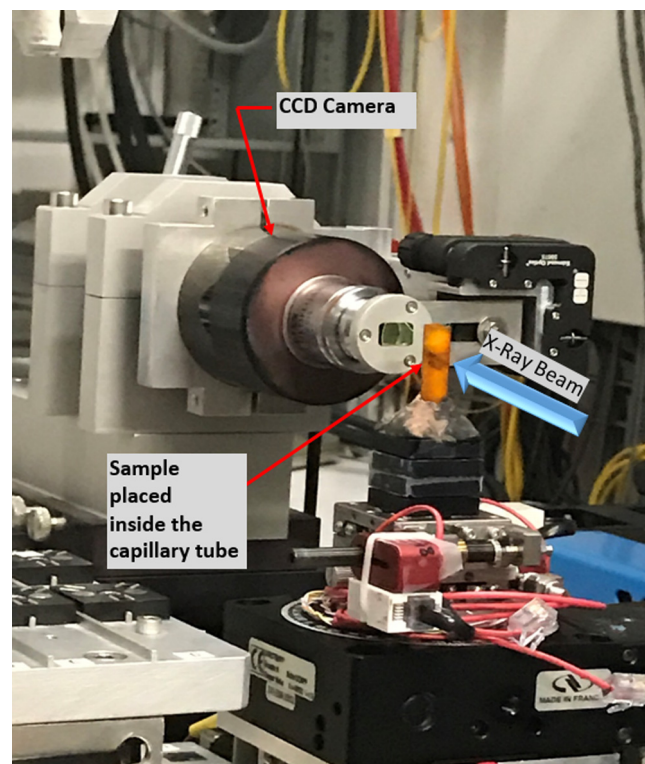


**Fig. 2.** Experimental set-up used at Beamline 2-BM at the Advanced Photon Source at Argonne National Laboratory, Illinois. The samples were fragments of the hardened cement past samples, which had been prepared as  $\sim 1$  mm length cubes.

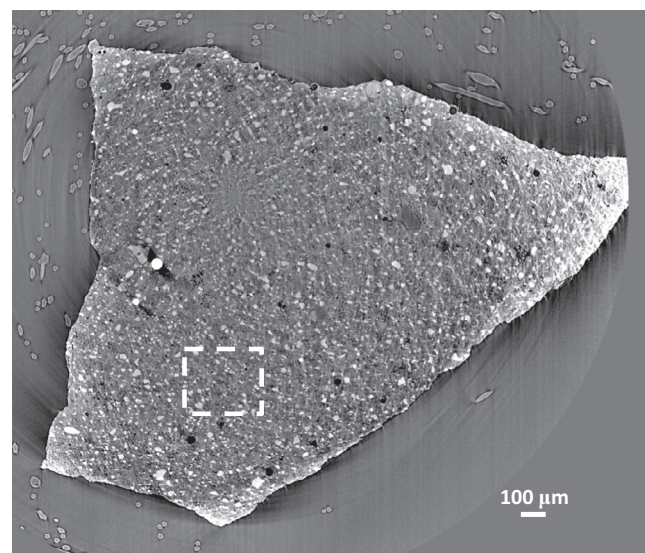


**Fig. 3.** A slice through the complete tomographic reconstruction of the OPC+FA-Ctrl sample.

#### 3.2. X-ray diffraction analysis

The XRD spectra for the four OPC samples (Ctrl, RP, LD, and HD) are shown in Fig. 5. As is commonly observed in hydrated OPC calcium silicate hydrate (C-S-H) phases were detected on all the samples. In addition, Portlandite, a crystalline form of calcium hydroxide, along with calcite was observed among the samples. The sulfate related phases that were present were thenardite and ettringite were detected among OPC sample. In addition, dolomites were detected among all the samples. Addition of high dose plastic

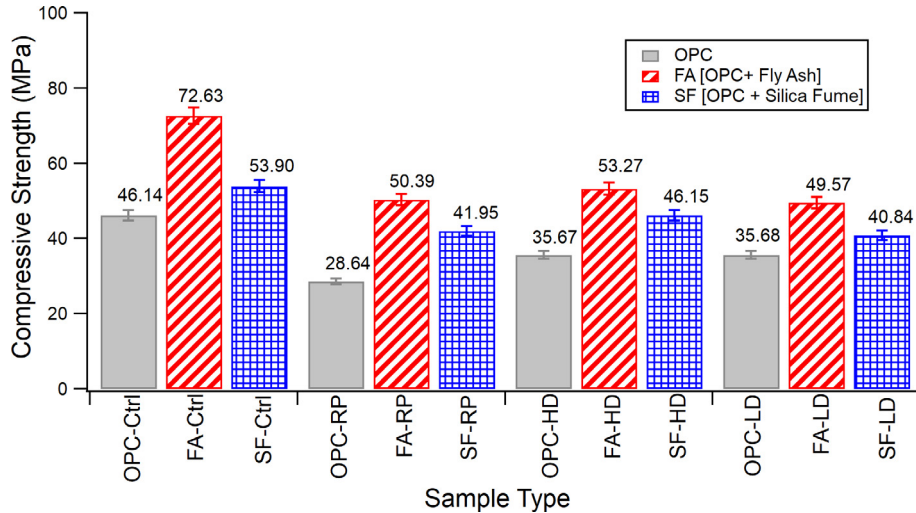


**Fig. 4.** Compressive strength analysis for all specimens. The bars represent the averages of the three samples for each combination. An increase of strength from regular plastic to high dose irradiated plastic is observed for all three cement binder types.

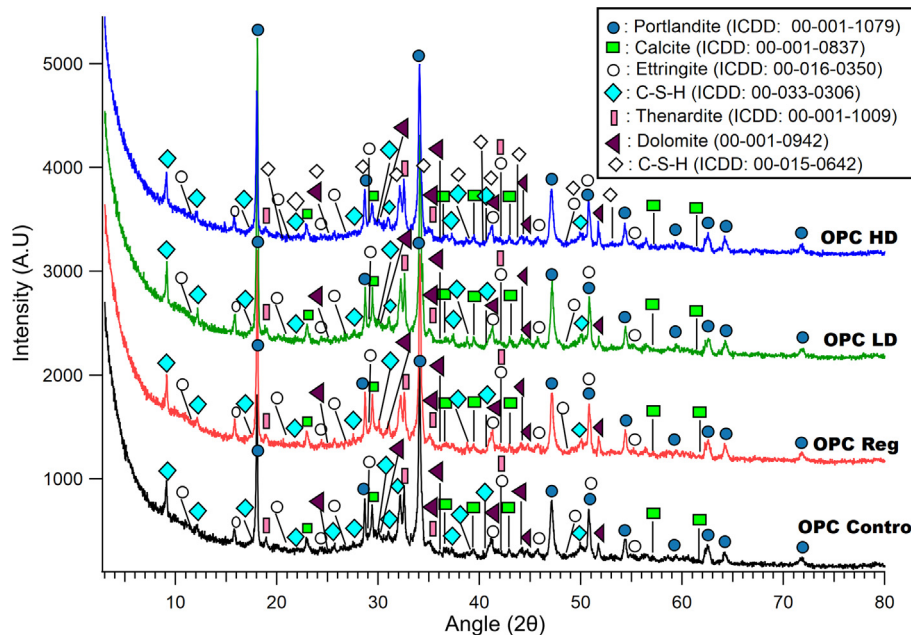


**Fig. 5.** XRD analysis for OPC samples prepared with regular, low dose, and high dose plastic. The gismondine phase was only present in the low dose sample.

led to the formation of different forms of C—S—H phases ( $\text{Ca}_{1.5}\text{SiO}_{3.5}\text{H}_2\text{O}$  ICDD: 00-033-0306;  $\text{Ca}_2\text{SiO}_4 \cdot 0.5\text{H}_2\text{O}$  ICDD: 00-015-0642) indicating that irradiation plastic at high dose can alter the crystal structure and chemical composition of C—S—H gels.

The XRD spectra for the four FA samples (Ctrl, RP, LD, HD) are shown in Fig. 6. Many of the same phases as in OPC were apparent since Portland cement was the main precursor for preparing the samples. The okenite phase, which is related to a zeolite type mineral, was only present in the FA-Ctrl sample. Okenite, an uncommon reaction product, has also been observed as one of the crystallization products for alkali silica reaction (ASR) gels (Guthrie and Carey, 2015). However, it cannot be confirmed given the phases apparent here that the presence of okenite led to any ASR gel formation. Furthermore, the addition of irradiated plastic allowed for different forms of C—A—S—H gel formation (chabazite-Ca were present), though in this case those phases were detected in the FA-Ctrl and FA-RP samples, as well.

The XRD spectra for the four OPC+SF samples (Ctrl, RP, LD, HD) are shown in Fig. 7. Again, many of the same phases as in OPC and FA samples were apparent. The presence of gismondine was detected only in the OPC+SF-LD and OPC+SF-HD samples. Thus irradiated plastic along with the addition of silica fume could have contributed to unique C—A—S—H gel formation. The gismondine phase, specifically, is attributed the storage of chemically bound water incorporating ions of calcium and silicon in small cages, which can later contribute to additional hydration and an increase in strength of the cement matrix along with the C—S—H gels (De Silva and Glasser, 1993). It is possible, then, that this effect explains the strength increase observed for the OPC+SF-HD sample as compared to the OPC+SF-RP sample.

In addition to differences within each binder type due to the various plastic additives, there were also distinct dissimilarities apparent in the comparison between OPC, OPC+FA, and OPC+SF. C—S—H type III was present only among the OPC samples, whereas

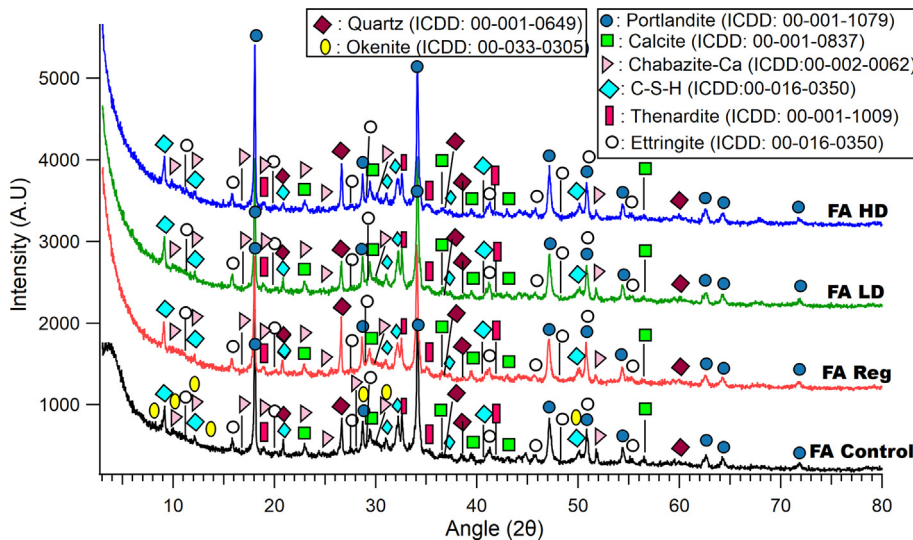


**Fig. 6.** XRD analysis for FA samples (OPC+FA) prepared with regular, low dose, and high dose plastic.

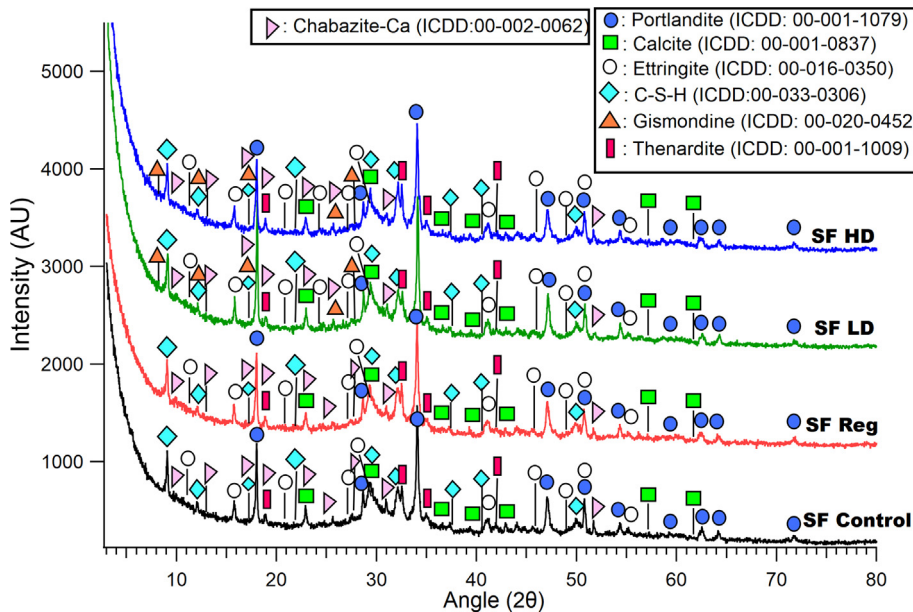


**Fig. 7.** XRD analysis for SF samples (OPC+SF) prepared with regular, low dose, and high dose plastic. The gismondine phase was only present in the low dose and high dose samples.

okenite was observed only in OPC+FA samples. Studies have shown that the presence of okenite is related to zeolite type mineral and its occurrence could have been due to the addition of fly ash. It is unclear, however, whether or not this occurred within the OPC +FA samples or if such an effect could have contributed to the observed strength increases resulting from the addition of fly ash.

### 3.3. Backscattered Electron (BSE) and ternary phase diagram analysis

BSE analysis on hardened polished samples for FA combinations is shown in Fig. 8. The advantage of BSE is the ability to achieve a wide range of magnifications in order to examine the individual hydration products (Scrivener et al., 2016; Scrivener, 2004). During the cement hydration process, the free water reacts with the clinker forming chemically bound water, which is formed in C–S–H gels. It can be seen in Fig. 8 that there is a water-filled outer space of C–S–H and calcium hydroxide crystals, along with alite ( $C_3S$ ). A central grain of belite ( $C_2S$ ) that is  $\sim 4 \mu m$  in size is also visible. It

shows the classic striations that arise from crystal twinning and that are highly temperature dependent (Scrivener, 2004). It is also important to note that the Portland cement powder contains pure  $C_3S$  (tricalcium silicate, or alite),  $C_2S$  (dicalcium silicate, or belite),  $C_3A$  (tricalcium aluminate), and  $C_4AF$  (tetracalcium aluminoferrite), but hydration forms these into impure forms. Thus the alites and belites pointed out in Fig. 8, which are products formed during hydration, are impure forms of these compounds.

Inclusion of fly ash led to spherical, unreacted fly ash particulates that may not have been involved in the hydration process. Fig. 8c shows that fly ash grains appear to be hollow, and it is possible that hydrates have filled inside the grains. Dark rims of magnesium containing hydrotalcite-like phases were also observed in these samples. The darker grey areas in the BSE image are made up of enriched carbon and oxygen, and they are attributed to carbonates.

EDS analysis was used to perform elemental and phase analysis for all samples. As an example, the results for the FA-LD sample are

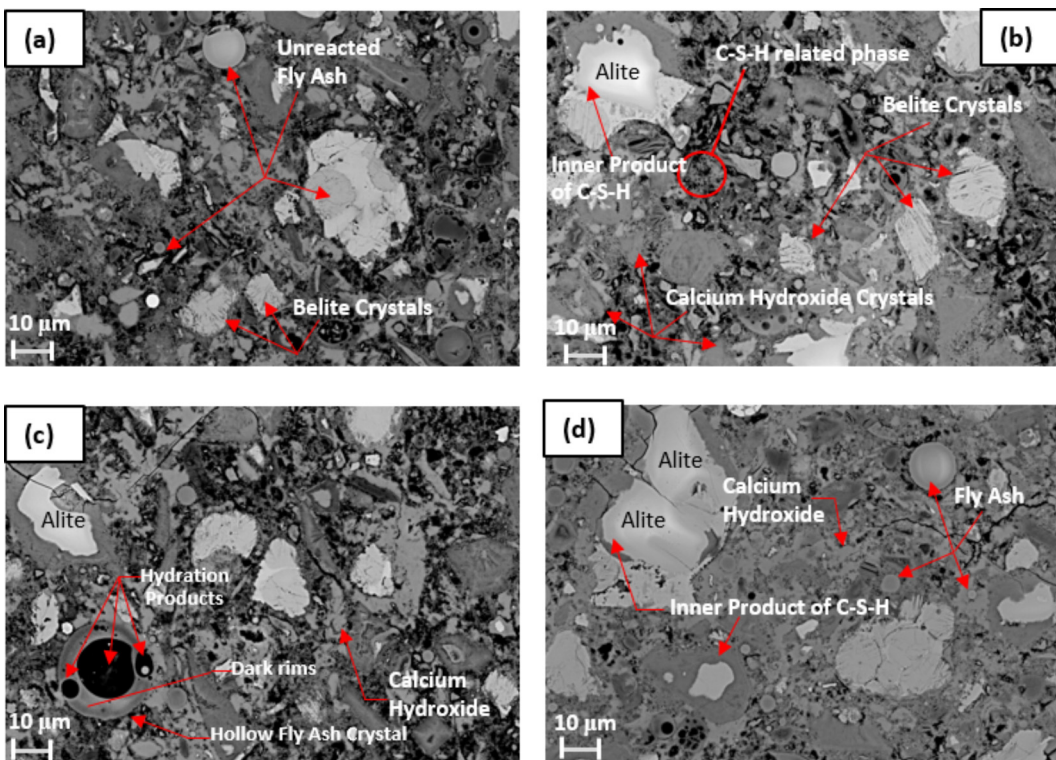


**Fig. 8.** BSE analysis on hardened polished samples of (a) FA-Ctrl, (b) FA-RP, (c) FA-LD, and (d) FA-HD.

shown in Fig. 9. The elemental analysis helps determine the distribution certain elements of interest, including oxygen, aluminum, calcium, and silicon, as shown in Fig. 9b. A fairly new technique developed within EDS shows a phase map which detects the phases and semi-quantitatively calculates the percentage of phase present in the hydrated sample. This analysis, depicted in Fig. 9c, can provide additional verification of the XRD studies that were reported in the Section 3.2.

Figs. 8 and 9 are included for visualization purposes; observation of BSE images and comparison of elemental- and phase-mapping among the different specimens can provide only a qualitative insight. A more definite comparison can be made visually with a ternary phase diagram, the use of which is a powerful technique for visualizing and predicting phase assemblages and relative phase contents using three chemical compositions (Herfort and Lothenbach, 2015). The oxide composition obtained via BSE for all samples was plotted as a CaO-Al<sub>2</sub>O<sub>3</sub>-SiO<sub>2</sub> ternary diagram and is shown in Fig. 10.

From the ternary phase diagram it can be noted that the addition of mineral additives (silica fume and fly ash) led to an increase in SiO<sub>2</sub> and a decrease in CaO. The OPC samples, therefore, can be classified as having high calcium content, whereas with FA and SF samples have medium calcium content. The data clearly indicates that the addition of SF increased the silica content, thereby increasing the formation of silicate in C-A-S-H gels, whereas the addition of fly ash formed C-A-S-H gel with higher alumina content. This suggests that the alumina content, in addition to the secondary C-S-H formed due to the addition of fly ash in Portland cements, helped to form the high-density phases that contributed to the higher relative strength among the FA samples.

#### 3.4. X-Ray Microtomography (X-Ray $\mu$ CT) analysis

For the purpose of illustration, a volume of interest (VOI) was obtained from the original data set of each specimen, as shown for

the OPC-LD sample in Fig. 11. As an example, the extracted volume is shown on a grey scale in Fig. 11a, where black color shows the pores and white represents the densest phase. Because pore detection is difficult on the grey scale shown, the VOI image was then transformed, as shown in Fig. 11b, in order to obtain the segmented porosity. This method involves separating the pore from the solid matrix by defining the range of grey scale—or, in this case, blue scale—that is associated with pore voxels. Here, segmented porosity refers to the extracted pore space after segmentation. Once segmented, pore connectivity can be revealed by determining whether or not adjacent pore voxels are in face-to-face contact and therefore connected to form a pore cluster. The percolating pore cluster is the largest pore cluster that permeates in three orthogonal directions (Promentilla et al., 2009). The percolating pore network relates to the effective porosity, as the interconnected part of the segmented porosity would most likely contribute to the ingress of species such as chlorides and sulfates in the pores of the cement matrix. In other words, it is assumed that the largest percolating pore cluster represents the connected pores that most likely facilitate macroscopic transport within the cement matrix. The largest percolating pore cluster is assumed to be the connected pores that most likely contribute to macroscopic transport in the cement matrix. This effective pore network is depicted in Fig. 11c. Thus the panels within Fig. 11 represent the intermediate stages of the porosity calculation.

The segmented porosities, obtained via a segmentation process using X-ray microtomography like the one described above, is shown in Fig. 12. OPC-RP exhibited the highest porosity (0.38), whereas the FA-Ctrl sample showed the least porosity (0.15). The results indicate that the addition of fly ash and silica fume led to decreases in porosity as compared to OPC samples, which showed the highest porosity values. It should be noted that the addition of high dose irradiated plastic contributed to a decrease in segmented porosity for all three binder types when compared to the samples with regular plastic (OPC-RP, FA-RP, SF-RP). It is worth noting that even though subtle differences were observed among the

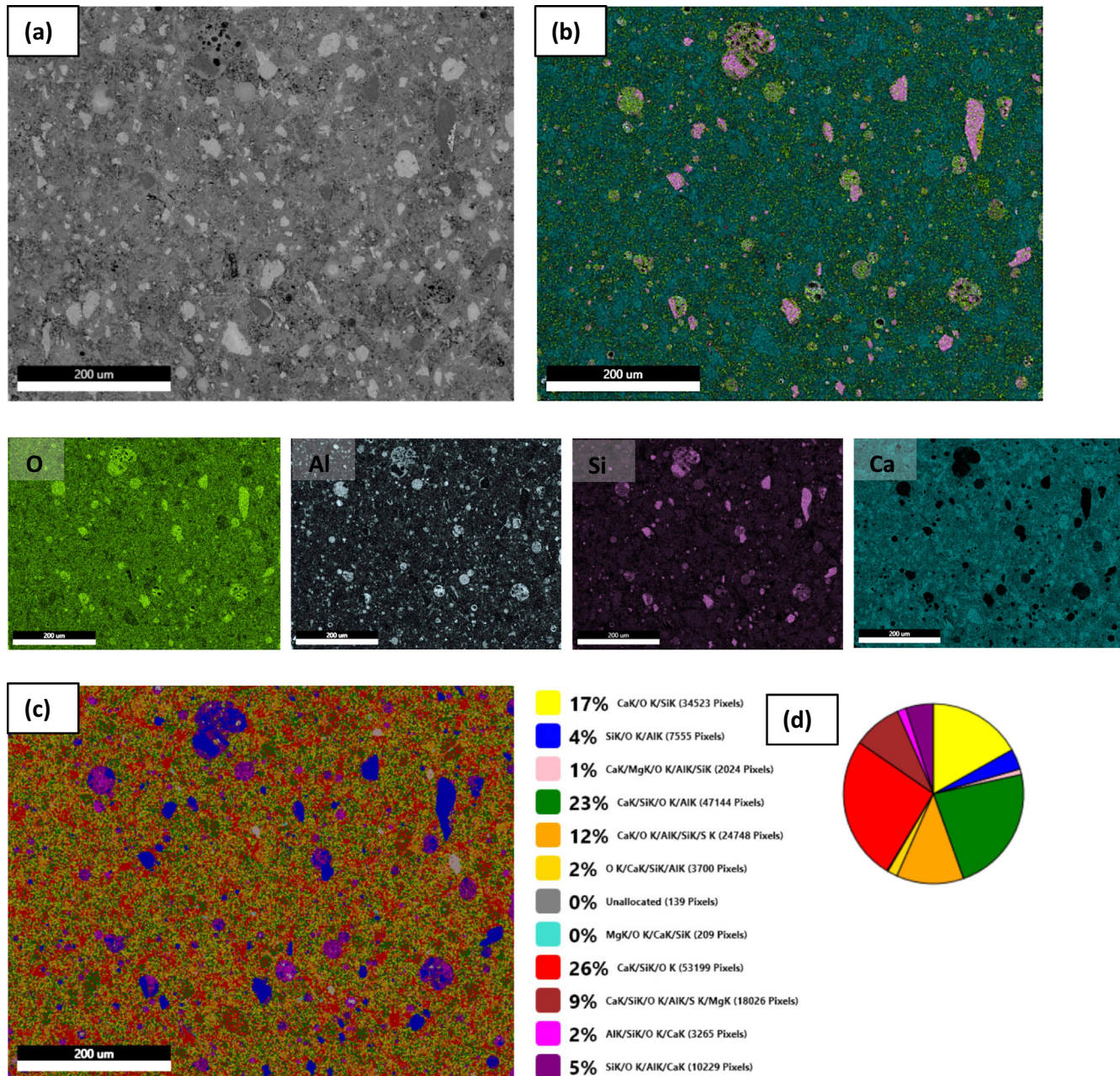


**Fig. 9.** BSE analysis of the FA-LD sample after 28 days of curing, including (a) BSE image, (b) elemental composition mapping, (c) phase composition mapping using EDS analysis, and (d) pie chart depiction of phase composition.

compressive strength values for OPC-LD, OPC-HD and FA-LD and FA-HD, variation in porosity was detected. This reduction in porosity is attributed to the variation in the crystal structure and phases which significantly affected the pore structure formation. For example, OPC-LD had only type of C—S—H phases, while inclusion of high dose plastic (OPC-HD) led to two different types of C—S—H gels, which may have contributed to additional densification of the resulting cementitious matrix. This suggests that inclusion of irradiated plastic may have acted as a pore-blocking agent, in addition to its formation of chemical phases such as C—S—H and C—A—S—H, which contributed to the densification of the cementitious matrix.

### 3.5. Summary of findings

Compression testing showed that a high dose irradiated plastic additive did indeed improve strength as compared to the regular

and non-irradiated plastic. This suggests that gamma irradiation is a viable potential solution for gaining back some of the strength that is lost when plastic is added to cement paste. It also highlights that irradiation of plastic helps to partially recover some part of the strength which was decreased due to addition of regular or non-irradiated plastic. XRD analysis showed that various differences in C—S—H and C—A—S—H phase formation from the addition of both irradiated plastic and mineral additives helped to form high-density phases that contributed to higher relative strength among the HD and LD samples. The discerning presence of the gismondine phase, in particular, suggests that the addition of irradiated plastic may have caused a change in the structure of C—S—H gels and initiated the possible formation of unique C—A—S—H gels. This could explain, in part, the strength increases shown in the irradiated plastic-containing samples. BSE analysis showed that a higher alumina content among fly ash samples

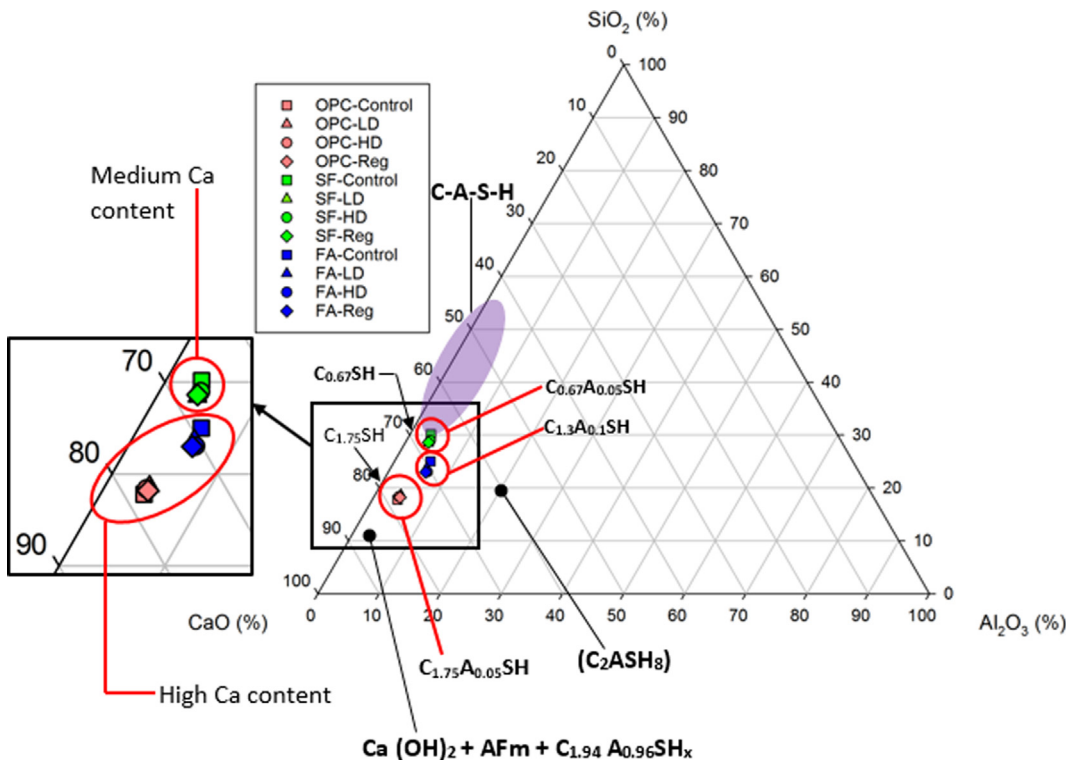


**Fig. 10.** Bulk composition obtained via Energy Dispersive Spectroscopy (EDS) analysis plotted onto the CaO–Al<sub>2</sub>O<sub>3</sub>–SiO<sub>2</sub> ternary diagram. CaO is plotted in the left-side axis, Al<sub>2</sub>O<sub>3</sub> on the bottom axis, and SiO<sub>2</sub> on the right-side axis.

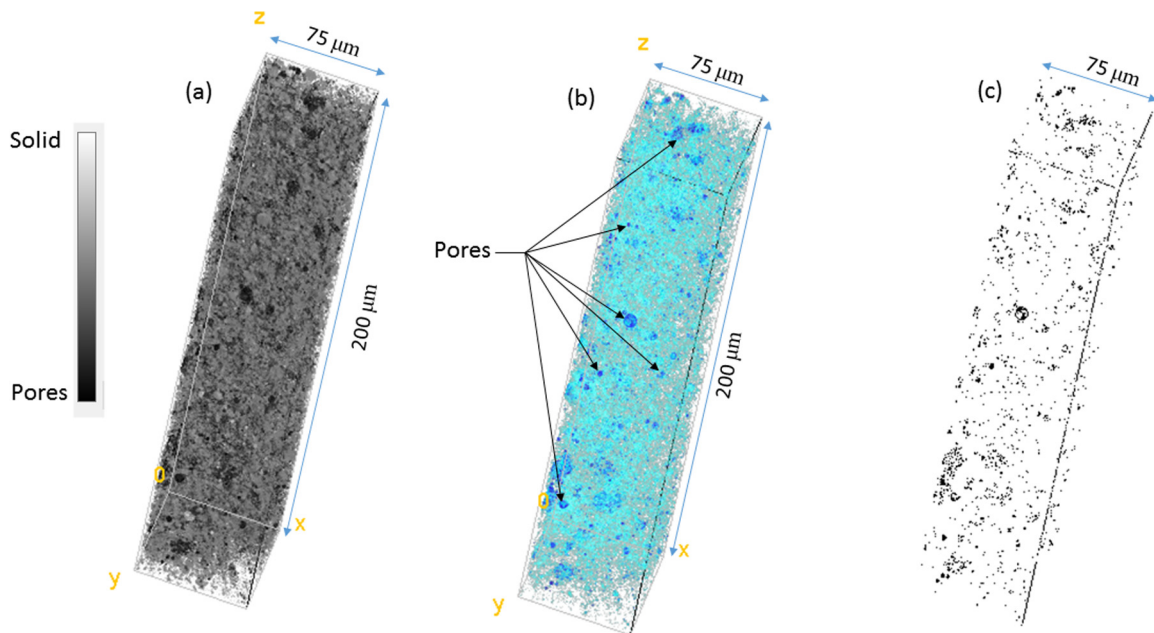


**Fig. 11.** X-ray microtomography analysis for the OPC-LD sample, including (a) extracted volume on a grey scale showing black as pores and white as solid, (b) detection of pores (blue color) in the sample that was used to obtain segmented porosity, and (c) effective pore network.

helped to form the high-density phases that contributed to higher relative strength among the fly ash samples, as evidenced in the ternary phase diagram. X-ray microtomography showed that the addition of high dose irradiated plastic consistently contributed to a decrease in segmented porosity, indicating that irradiated plastic may have acted as a pore-blocking agent. This effect is in addition to its formation of chemical phases such as C–S–H and

C–A–S–H, which contributed to the densification of the cementitious matrix.

To date, limited studies have been performed to understand the chemo-mechanical and microstructure aspect when irradiated plastics are used for permanent waste disposal along with partial recovery of mechanical properties in Portland cements. A micro and pore-structural insight using multi-scale length techniques

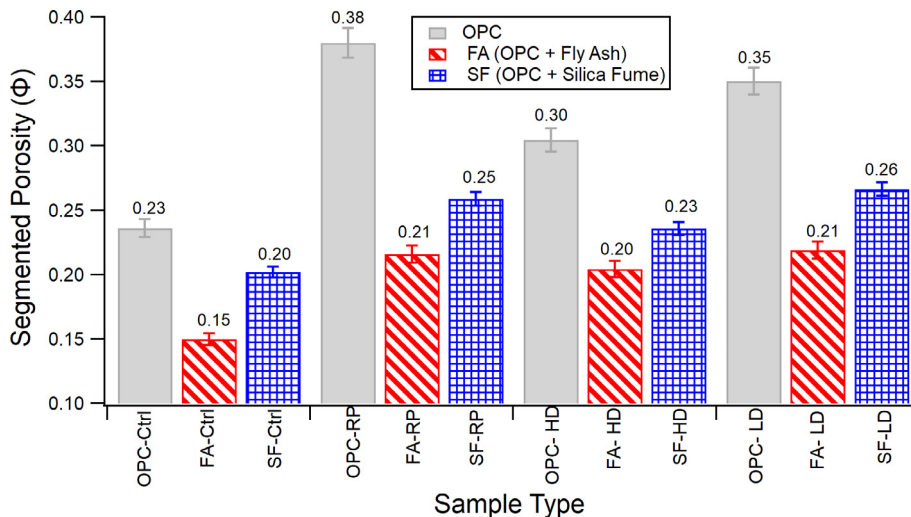


**Fig. 12.** Segmented porosity obtained from X-ray microtomography data for all the samples. Samples containing FA or SF showed lower levels of porosity than did OPC samples. For all three cement binder types, the HD samples showed lower levels of porosity than did the RP samples.

(XRD: nm, BSE/EDS:  $\mu\text{m}$ ; Tomography:  $\mu\text{m}$ ) will provide the necessary insight for a successful use of irradiated plastics over regular plastics in the concrete/cement industry. Moreover, this approach can be incorporated in developing new codes and standards when irradiated plastic along with supplementary cementitious materials (SCM's) are used for developing engineered cements for the 21st century.

#### 4. Conclusions

This study clearly showed the benefits of using gamma irradiated recycled plastic in place of unirradiated plastic to partially recover the strength of Portland cement, while simultaneously displacing cement volume, reducing its carbon footprint without associated drawbacks. A thorough micro- and pore-structural analysis was performed in order to provide insight at an angstrom-level scale (through XRD) and at a micron-level scale (through BSE and microtomography). It was determined that incorporating high dose irradiated plastic along with SCM's into cement paste samples led to decreased porosity and increased compressive strength, which was attributed to the formation of C—A—S—H gels along with secondary C—S—H, which forms during the hydration processes.

By partially replacing Portland cement with a recycled waste plastic, this design may have a potential to contribute to reduced carbon emissions when scaled to the level of mass concrete production. Based on comparison with previous studies that used recycled plastic as an additive, it is clear that irradiation adds the benefit of increased compressive strength. Further research should be done to discover the true optimal combination of irradiated plastic and mineral additive for high strength. The groundwork, however, has been laid for the continued development of the ideas presented here.

#### Acknowledgement

Use of the Advanced Photon Source (APS), an Office of Science User Facility operated for the U.S. Department of Energy (DOE) Office of Science by Argonne National Laboratory, was supported by the U.S. DOE under Contract No. DE-AC02-06CH11357. We would like to thank Jim Wolsiefer from Norchem, Inc. and Dr. Ivan Diaz Loya from Headwater Resources for providing the silica fume and fly ash, respectively, for this project. We acknowledge Mark Croyle from Evergreen Plastics for providing the PET flakes.

Many thanks to Peter Brenton and the MIT Department of Nuclear Science and Engineering for their financial support, Mitch Galanek and Ryan Samz from MIT EHS for assistance with access to and use of the cobalt-60 facility. We also thank Stephen Rudolph for help with compression testing, Dr. Charlie Settens for help in XRD analysis, and Patrick Boisvert from the MIT Center for Materials Science and Engineering (CMSE), a U.S. National Science Foundation (NSF) Materials Research Science & Engineering Center (MRSEC), for assisting with the BSE analysis. All specimen preparation, mechanical testing and data analysis were performed at the Laboratory for Infrastructure Science and Sustainability (LISS) in the Department of Civil and Environmental Engineering of MIT.

#### Appendix A. Justification of plastic percent composition

A constraint on the total number of samples that could be set and tested necessitated the selection of one ideal percent composition of plastic in the cement samples. Previous studies were reviewed in order to determine the composition at which plastic-enhanced concrete displays maximum strength. The findings are summarized in Table A1. The given references can be found in the References section of this paper. Past research showed a general decrease in strength as the percent composition increased.

**Table A1**

Literature review for selection of percent plastic composition.

Polymer added to cement	Percentage metric	Strength type(s)	Trend	Reference number
Not specified (general plastic)	Weight	Compressive, flexural, tensile	Steady decrease up to 20%	Batayneh et al. (2007)
Polyethylene terephthalate	Volume	Compressive	Maximum at 1%	Nibudey et al. (2013)
Not specified (general plastic)	Weight	Compressive	Steady decrease up to 15%	Rai et al. (2012)
Polyethylene terephthalate	Volume	Compressive, tensile	(Comp) steady decrease up to 50%, (tens) maximum at 1.5%	Hannawi et al. (2010)
Polycarbonate	Volume	Compressive, tensile	Steady decrease up to 50%	Hannawi et al. (2010)

**Table A2**

Literature review for selection of high and low dose levels.

Polymer	Strength type	Trend	Maximum strength increase	Reference number
Polyethylene	Tensile	Increases up to 10 kGy	Not specified	Plester (1973)
Polyethylene	Impact	Begins to fall at 70 kGy	Not specified	Plester (1973)
Polyethylene terephthalate	Tensile	Increases up to 150 kGy	Not specified	Martínez-Barrera et al. (2015)
Polyethylene terephthalate	Compressive	Increases up to 100 kGy	35%	Martínez-Barrera et al. (2015)
Polyethylene terephthalate	Mechanical	Increases up to 200 kGy	50%	Martínez-Barrera et al. (2015)
Polyethylene terephthalate	Tensile	Increases up to 10 kGy	6%	Jeon et al. (2004)
Polyethylene terephthalate	Tensile	Maximum at 60 and 105 kGy	19%	Oliveira et al. (2009)

No strength improvements were observed for plastic compositions beyond 1.5% by volume. For this study, a 1.25% composition by weight was chosen.

## Appendix B. Justification of dose levels for plastic additive

Previous studies were reviewed in order to determine the dose levels for the irradiated plastic additive. Trends in strength with varying dose according to different studies are summarized in **Table A2**. The given references can be found in the References section of this paper. The irradiation type used in the study represented by the last row was electron-beam irradiation, while all others used gamma irradiation. The results for PET are somewhat inconsistent and suggest a need to test both high and low dose levels. A low dose and high dose of 10 kGy and 100 kGy, respectively, were selected for the testing in this study.

## References

- Al-Salem, S.M., Lettieri, P., Baeyens, J., 2009. Recycling and recovery routes of plastic solid waste (PSW): a review. *Waste Manage.* 29, 2625–2643.
- Ali, M.B., Saidur, R., Hossain, M.S., 2011. A review on emission analysis in cement industries. *Renew. Sustain. Energy Rev.* 15, 2252–2261.
- Alqahtani, F.K., Ghataora, G., Khan, M.I., Dirar, S., 2017. Novel lightweight concrete containing manufactured plastic aggregate. *Constr. Build. Mater.* 148, 386–397.
- Andres, R.J., Marland, G., Fung, I., Matthews, E., 1996. A  $1^\circ \times 1^\circ$  distribution of carbon dioxide emissions from fossil fuel consumption and cement manufacture, 1950–1990. *Glob. Biogeochem. Cycles* 10, 419–429.
- Asokan, P., Osmanli, M., Price, A.D.F., 2010. Improvement of the mechanical properties of glass fibre reinforced plastic waste powder filled concrete. *Constr. Build. Mater.* 24, 448–460.
- ASTM-C39, 2016. ASTM C-39, Standard Test Method for Compressive Strength of Cylindrical Concrete Specimens. ASTM International.
- ASTM-C109, 2016. Standard Test Method for Compressive Strength of Hydraulic Cement Mortars (Using 2-in. or [50-mm] Cube Specimens). ASTM International, West Conshohocken, PA, pp. 1–10.
- ASTM, 2004. ASTM C 618 Standard Specification for Coal Fly Ash and Raw or Calcined Natural Pozzolans for Use as a Mineral Admixture in Concrete. Annual Book of ASTM Standard, Section 4.
- ASTM, 2014. ASTM 305-14Standard Practice for Mechanical Mixing of Hydraulic Cement Pastes and Mortars of Plastic Consistency, ASTM C305-14. ASTM International, West Conshohocken, p. 3.
- Ávila Córdoba, L., Martínez-Barrera, G., Barrera Díaz, C., Ureña Nuñez, F., Loza Yáñez, A., 2013. Effects on mechanical properties of recycled PET in cement-based composites. *Int. J. Polym. Sci.* 2013, 1–6.
- Batayneh, M., Marie, I., Asi, I., 2007. Use of selected waste materials in concrete mixes. *Waste Manage.* 27, 1870–1876.
- Choi, Y.-W., Moon, D.-J., Chung, J.-S., Cho, S.-K., 2005. Effects of waste PET bottles aggregate on the properties of concrete. *Cem. Concr. Res.* 35, 776–781.
- Choi, Y.W., Moon, D.J., Kim, Y.J., Lachemi, M., 2009. Characteristics of mortar and concrete containing fine aggregate manufactured from recycled waste polyethylene terephthalate bottles. *Constr. Build. Mater.* 23, 2829–2835.
- Colangelo, F., Cioffi, R., Liguori, B., Iucolano, F., 2016. Recycled polyolefins waste as aggregates for lightweight concrete. *Compos. B Eng.* 106, 234–241.
- Coppola, B., Courard, L., Michel, F., Incarnato, L., Di Maio, L., 2016. Investigation on the use of foamed plastic waste as natural aggregates replacement in lightweight mortar. *Compos. B Eng.* 99, 75–83.
- Corbett, J.J., Fischbeck, P., 1997. Emissions from ships. *Science* 278, 823–824.
- Crow, J.M., 2008. The concrete conundrum. *Chem. World* 5, 62–66.
- De Silva, P.S., Glasser, F.P., 1993. Phase relations in the system  $\text{CaO}-\text{Al}_2\text{O}_3-\text{SiO}_2-\text{H}_2\text{O}$  relevant to metakaolin – calcium hydroxide hydration. *Cem. Concr. Res.* 23, 627–639.
- Demirel, B., Yaras, A., Elçiçek, H., 2016. Crystallization behavior of PET materials. *Balıkesir Üniversitesi Fen Bilimleri Enstitüsü Dergisi* 13, 26–35.
- EPA, 2014. Municipal Solid Waste Generation, Recycling, and Disposal in the United States Tables and Figures for 2012. Environmental Protection Agency, pp. 1–63.
- Gesoglu, M., Güneyisi, E., Hansu, O., Etili, S., Alhassan, M., 2017. Mechanical and fracture characteristics of self-compacting concretes containing different percentage of plastic waste powder. *Constr. Build. Mater.* 140, 562–569.
- Gu, L., Ozbaikoglu, T., 2016. Use of recycled plastics in concrete: a critical review. *Waste Manage.* 51, 19–42.
- Guthrie, G.D., Carey, J.W., 2015. A thermodynamic and kinetic model for paste-aggregate interactions and the alkali-silica reaction. *Cem. Concr. Res.* 76, 107–120.
- Hannawi, K., Kamali-Bernard, S., Prince, W., 2010. Physical and mechanical properties of mortars containing PET and PC waste aggregates. *Waste Manage.* 30, 2312–2320.
- Herfort, D., Lothenbach, B., 2015. Ternary Phase Diagrams Applied to Hydrated Cement, A Practical Guide to Microstructural Analysis of Cementitious Materials. CRC Press, pp. 485–502.
- Iucolano, F., Liguori, B., Caputo, D., Colangelo, F., Cioffi, R., 2013. Recycled plastic aggregate in mortars composition: effect on physical and mechanical properties. *Mater. Des.* 1980–2015 (52), 916–922.
- Jeon, D.H., Lee, K.H., Park, H.J., 2004. The effects of irradiation on physicochemical characteristics of PET packaging film. *Radiat. Phys. Chem.* 71, 1059–1064.
- Jog, J.P., 1995. Crystallization of polyethyleneterephthalate. *J. Macromol. Sci. Part C* 35, 531–553.
- Kattan, M., 2006. Thermal behavior of gamma-irradiated amorphous poly(ethylene terephthalate) films. *Polym. Eng. Sci.* 46, 1374–1377.
- Kim, S.B., Yi, N.H., Kim, H.Y., Kim, J.-H.J., Song, Y.-C., 2010. Material and structural performance evaluation of recycled PET fiber reinforced concrete. *Cem. Concr. Compos.* 32, 232–240.
- Klug, H.P., Alexander, L.E., 1974. X-Ray Diffraction Procedures: For Polycrystalline and Amorphous Materials. Wiley.
- Li, Z., 2011. Advanced Concrete Technology. Wiley.
- Martínez-Barrera, G., Ávila-Córdoba, L.I., Martínez-López, M., Herrera-Sosa, E.S., Santiago, E.V., Barrera-Díaz, C.E., Ureña-Nuñez, F., González-Rivas, N., 2015. Gamma radiation as a recycling tool for waste materials used in concrete. In: Nenoj, M. (Ed.), Evolution of Ionizing Radiation Research. InTech, Rijeka. Chapter 11.
- Martínez-Barrera, G., Menchaca-Campos, C., Hernández-López, S., Vigueras-Santiago, E., Brostow, W., 2006. Concrete reinforced with irradiated nylon fibers. *J. Mater. Res.* 21, 484–491.
- Martínez-Barrera, G., Ureña-Nuñez, F., Gencel, O., Brostow, W., 2011. Mechanical properties of polypropylene-fiber reinforced concrete after gamma irradiation. *Compos. A Appl. Sci. Manuf.* 42, 567–572.
- Martínez-Barrera, G., Vigueras-Santiago, E., Hernández-López, S., Brostow, W., Menchaca-Campos, C., 2005. Mechanical improvement of concrete by irradiated polypropylene fibers. *Polym. Eng. Sci.* 45, 1426–1431.
- Marzouk, O.Y., Dheilly, R.M., Queneudec, M., 2007. Valorization of post-consumer waste plastic in cementitious concrete composites. *Waste Manage.* 27, 310–318.
- Muhit, I., Ahmed, S., Amin, M., Raihan, M., 2013. Effects of silica fume and fly ash as partial replacement of cement on water permeability and strength of high performance concrete. In: 4th International Conference on Advances in Civil Engineering, AETACE, Association of Civil and Environmental Engineers.
- Neville, A.M., 2011. Properties of Concrete. Prentice Hall PTR.
- Nibudey, R., Nagarnaik, P., Parbat, D., Pande, A., 2013. A model for compressive strength of PET fiber reinforced concrete. *Am. J. Eng. Res.* 2, 367–372.
- Oliveira, V.M., Ortiz, A.V., Del Mastro, N.L., Moura, E.A.B., 2009. The influence of electron-beam irradiation on some mechanical properties of commercial multilayer flexible packaging materials. *Radiat. Phys. Chem.* 78, 553–555.
- Pelisser, F., Montedo, O.R.K., Gleize, P.J.P., Roman, H.R., 2012. Mechanical properties of recycled PET fibers in concrete. *Mater. Res.* 15, 679–686.
- Plester, D.W., 1973. The Effects of Radiation Sterilization on Plastics, Industrial Sterilization. Duke University Press, pp. 141–152.
- Promentilla, M.A.B., Sugiyama, T., Hitomi, T., Takeda, N., 2009. Quantification of tortuosity in hardened cement pastes using synchrotron-based X-ray computed microtomography. *Cem. Concr. Res.* 39, 548–557.
- Rai, B., Rushad, S.T., Kr, B., Duggal, S.K., 2012. Study of waste plastic mix concrete with plasticizer. *ISRN Civ. Eng.* 2012, 5.
- Roy, D.M., Arjunan, P., Silsbee, M.R., 2001. Effect of silica fume, metakaolin, and low-calcium fly ash on chemical resistance of concrete. *Cem. Concr. Res.* 31, 1809–1813.

- Saikia, N., Brito, J.D., 2013. Waste polyethylene terephthalate as an aggregate in concrete. *Mater. Res.* 16, 341–350.
- Saikia, N., de Brito, J., 2012. Use of plastic waste as aggregate in cement mortar and concrete preparation: a review. *Constr. Build. Mater.* 34, 385–401.
- Scrivener, K., Snellings, R., Lothenbach, B., 2016. A Practical Guide to Microstructural Analysis of Cementitious Materials. Taylor & Francis.
- Scrivener, K.L., 2004. Backscattered electron imaging of cementitious microstructures: understanding and quantification. *Cem. Concr. Compos.* 26, 935–945.
- Siddique, R., Khatib, J., Kaur, I., 2008. Use of recycled plastic in concrete: a review. *Waste Manage.* 28, 1835–1852.
- Singh, N., Hui, D., Singh, R., Ahuja, I.P.S., Feo, L., Fraternali, F., 2017. Recycling of plastic solid waste: a state of art review and future applications. *Compos. B Eng.* 115, 409–422.
- Tanaka, N., Stigson, B., 2009. Cement Technology Roadmap: Carbon emissions reductions up to 2050, pp. 1–36.
- Taylor, H.F.W., 1997. *Cement Chemistry*. Thomas Telford.
- Varlashkin, P., 2011. Approaches to quantification of amorphous content in crystalline drug substance by powder X-ray diffraction. *Am. Pharmaceut. Rev.* 14.
- Worrell, E., Price, L., Martin, N., Hendriks, C., Meida, L.O., 2001. Carbon dioxide emissions from the global cement industry 1. *Annu. Rev. Energy Env.* 26, 303–329.
- Yoshida, A., 2005. China: The world's largest recyclable waste importer. *World* 3, 4–500.